Lateral critical current distribution and self-field profile of Bi-2223/Ag conductors: measurements and calculations

2006 Supercond. Sci. Technol. 19 848

(http://iopscience.iop.org/0953-2048/19/8/028)

INSTITUTE OF PHYSICS PUBLISHING SUPERCONDUCTOR SCIENCE AND TECHNOLOGY
Supercond. Sci. Technol. **19** (2006) 848–853 doi:10.1088/0953-2048/19/8/028

Lateral critical current distribution and self-field profile of Bi-2223/Ag conductors: measurements and calculations

E Demencik[1,4], **P Usak**[1], **M Polak**[1], **H Piel**[2] **and M Dhalle**[3]

[1] Institute of Electrical Engineering, Slovak Academy of Sciences, Dúbravska cesta 9, 841 04 Bratislava, Slovakia
[2] Cryoelectra GmbH, Linde 72, 42287 Wuppertal, Germany
[3] Department of Applied Physics, Low Temperature Division, University of Twente, PO Box 217, 7500AE Enschede, The Netherlands

E-mail: eduard.demencik@savba.sk

Received 11 May 2006, in final form 14 June 2006
Published 3 July 2006
Online at stacks.iop.org/SUST/19/848

Abstract
The lateral current distribution and the magnetic self-field induced by a transport current were measured independently in three multifilament Bi-2223/Ag tapes with qualitatively different filament layouts. The current and field data from these two experiments, magnetic knife and scanning Hall probe, are compared with each other after straightforward 'forward' or 'inverse' current-to-field calculations. Both datasets show the critical current to be maximal in the central part of the tapes, while the comparison demonstrates that the drop of the critical current distribution at the tape edges is an intrinsic material property and is not caused by the tape's magnetic self-field. Small differences between the datasets reveal the effect of filament bridging.

(Some figures in this article are in colour only in the electronic version)

1. Introduction

The main goal of this work is to determine the local lateral critical current distribution in three Bi-2223/Ag tapes at 77 K. Two tapes have a filament layout which is typical for commercial conductors, but different degrees of filament bridging. The third sample has a columnar filament arrangement and serves as a model system. Over the last decade, several strategies have been developed to study the local current distribution in tape-like HTS conductors. Two types of experiment can be distinguished: either the magnetic self-field generated by the current distribution is measured (see e.g. the review [1]) or current is confined to a selected part of the sample and the local critical current is measured directly. The latter experiment can be destructive [2] or non-destructive [3]. We use both a confinement and a magnetic type of experiment: the magnetic knife (MK) [3] yields the current distribution directly, while a Hall probe mapping system (HPMS) [4] measures the self-field profile above the current-carrying tapes (figure 1). As demonstrated in [4] and discussed below, the two types of experiments are complimentary in the sense that they characterize the current distribution under different geometrical and electro-magnetic constraints, so that a comparison between them yields extra information. Just like in [4], we used the MK data to calculate the expected self-field profile (forward calculation) and compared this to the actual self-field measured by the HPMS. However, in addition we also followed the inverse procedure, deducing the transport current distribution starting from the HPMS data (inverse calculation), and compare the result with the MK data.

In general, one cannot expect that the comparison between MK and HPMS data will yield identical results, since quite different experimental conditions apply to both. The first difference is the role of self-field suppression of J_c. In the HPMS experiment, the tapes are saturated with a transport current and the external field is zero. The perpendicular component of the self-field is maximal at the tape edges, which locally reduces the current-carrying capacity. In the

[4] Author to whom any correspondence should be addressed.

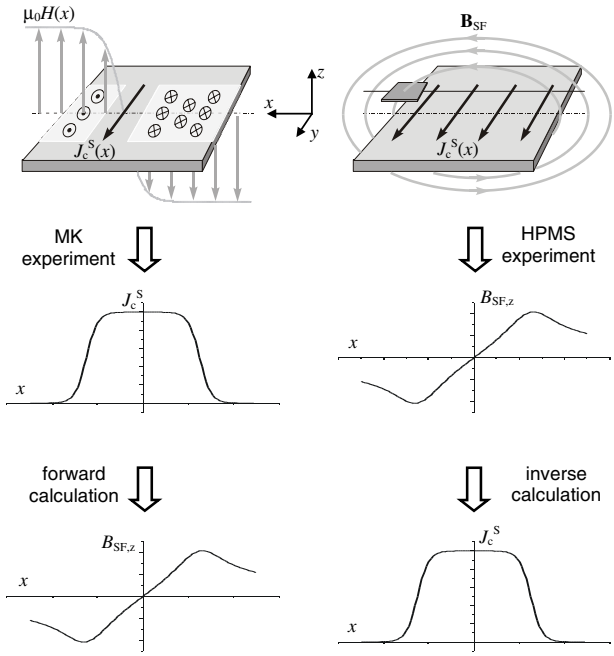

Figure 1. Schematic representation of the magnetic knife (MK, left) and scanning Hall probe (HPMS, right) experiments. The MK restricts the current to a narrow longitudinal channel and measures the lateral current distribution directly. The HPMS maps the perpendicular component of the self-field generated by a transport current. Both can be compared after forward or inverse calculation.

MK experiments, a relatively high external magnetic field is applied to most of the tape and the transport current is limited to a narrow region, so that self-field effects are negligible. Therefore, the critical current distribution measured by the MK will correspond to intrinsic variations of J_c, while the distribution deduced from the HPMS data will reflect both intrinsic and field-induced variations [5].

The second main difference has to do with current 'meandering' and filament bridging. In the MK experiment, the current is forced to flow through a narrow channel in the axial direction of the tape (y-direction, see figure 1), while the transport current in the HPMS measurements is free to flow also in the x-direction and can thus 'bypass' weaker spots by redistributing itself within and between filaments.

2. Experimental details

2.1. Samples

We used three multi-filamentary Bi-2223/Ag tapes in this work. The cross-sectional micrographs of the multifilament samples are shown in figures 2–4. The properties of the tapes are given in table 1.

Sample A, figure 2, is a typical Bi-2223/Ag multifilament tape with high spatial density of filaments and numerous inter-filamentary superconducting bridging; in sample B, figure 3, bridging is minimized due to a lower superconducting filling factor. Sample C, figure 4, has a special architecture of two separated columns, each containing eight stacked filaments. From the point of view of current distribution in the tapes, the geometry of sample B is the best defined one, since the current

Table 1. Characteristic parameters of the samples.

Sample	Size (mm)	No. of filaments	I_c (A)	Note
A	0.25 × 3.7 × 50	55	54	High density of filaments, filamentary bridging, not twisted
B	0.3 × 4.15 × 50	37	16	Low fill. factor, slight bridging expected, not twisted
C	0.25 × 3.4 × 50	16	17	16 filaments in 2 columns 2 × 8, not twisted

can barely meander between adjacent filaments (in contrast to samples A and C) and super-currents preferentially flow along individual filaments.

2.2. Direct critical current distribution determination—magnetic knife method

The MK [3] uses a step-like external magnetic field profile to suppress super-currents over most of the tape width and measures the critical current in the remaining low-field channel (figure 1). The amplitude of the applied field in our experiments is 0.427 T, except for an approximately 1 mm wide region, where magnetic field crosses zero and changes polarity to −0.427 T with a gradient of $\sim\Delta B/\Delta x = 1.12\ \mathrm{T\,mm^{-1}}$. The critical current is measured by the standard four-probe method using the electric field criterion $E_c = 1\ \mu\mathrm{V\,cm^{-1}}$. The distance between the voltage taps is ∼10 mm. The length of the iron cores that shape the step profile (20 mm along the tape) is long compared to the voltage tap distance. The external magnetic field profile is moved from one tape edge to the other with steps of $\Delta x = 50\ \mu$m. For each step, the critical current I_{cm} of the low-field channel is measured. These 'raw' $I_{cm}(x)$ data then have to be processed with a de-convolution procedure. With the standard fast Fourier transform (FFT) routines implemented in the Matlab software package, we used the convolution theorem according to which convolution in the 'time' domain corresponds with multiplication in the 'frequency' domain and vice versa, [6]:

$$I_{c,m}(x) = \int_{-\infty}^{-\infty} J_c(x')t(x')F(x-x')\,\mathrm{d}x'$$
$$\mathrm{FFT}(I_{c,m}) = \mathrm{FFT}(J_c t)\cdot\mathrm{FFT}(F) \qquad (1)$$
$$J_c^S \equiv J_c t = \mathrm{IFFT}\left[\frac{\mathrm{FFT}(I_{c,m})}{\mathrm{FFT}(F)}\right].$$

The de-convoluted quantity is the critical sheet current density $J_c^S(x)$, i.e. the critical current per unit tape width. It is equal to the total thickness (in the z-direction) $t(x)$ of the filaments at position x, multiplied by the average critical current density $J_c(x)$. The kernel $F(x)$ describes the external magnetic field profile $\mu_0 H(x)$ combined with the normalized overall $J_c(B)$ dependence of the tape:

$$F(x) = f[\mu_0 H(x)]; \qquad f(B) = J_c(B)/J_c(0). \qquad (2)$$

The functions $\mu_0 H(x)$ and $f(B)$ in (2) are measured separately and expressed by analytical formulae.

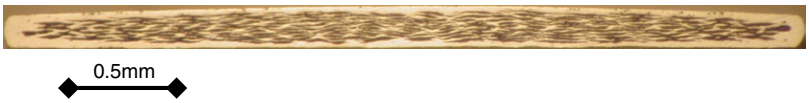

Figure 2. Cross-sectional micrograph of the Bi-2223/Ag tape A, which is typical for commercial conductors. The thickness of the tape is stretched unproportionally to show the filament layout.

Figure 3. Cross-sectional micrograph of tape B with less filaments and a lower superconducting fill factor. The thickness of the tape is stretched unproportionally to show the filament layout.

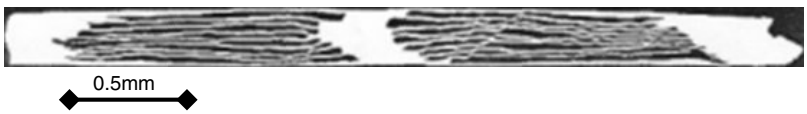

Figure 4. Cross-sectional micrograph of the columnar tape C, used as a test sample. The thickness of the tape is stretched unproportionally to show the filament layout.

2.3. Indirect current distribution determination—magnetic field mapping

The HPMS set-up is equipped with a Hall sensor that measures the component of magnetic field perpendicular to the sensor surface, B_z, figure 1. The active area of the sensor is 50 μm by 50 μm; its sensitivity is $\sim$170 mV T^{-1}. For the magnetic self-field measurements, the samples were supplied with a transport current corresponding to the full critical current (determined with the four-point method using an electric field criterion $E_c = 1\ \mu\text{V cm}^{-1}$). The field was mapped above the tape at a distance z of about two to three times the tape thickness ($z \approx 0.5$ mm).

For the calculation of the inverse problem (see below), the z-component of the self-field $B_{\text{SF},z}(x)$ was determined at 25 spatial points across the tape. This resolution is sufficient to resolve the current distribution across the tape, especially when considering the excellent measurement precision of the magnetic self-field component perpendicular to the tape (relative uncertainty better than 0.5%), which is much higher than the typical precision of magneto-optical methods.

2.4. Forward calculations

The magnetic field profiles corresponding to the measured MK critical current profiles were calculated in a forward way using equation (3), which gives the perpendicular component H_z of the field generated by a current I flowing uniformly distributed in an infinitely long strip of width w. The thickness of the strip is assumed to be negligibly small in comparison with all other dimensions [7].

$$H_z = -\frac{I}{2\pi w} \ln\left(\frac{r_1}{r_2}\right) \tag{3}$$

$r_{1,2}$ are the distances from the strips edges to the point where the field is calculated (figure 5). The calculation model consists of N such narrow strips placed in parallel. Each point of the magnetic self-field profile is then calculated as the sum of N contributions of all the sub-strips.

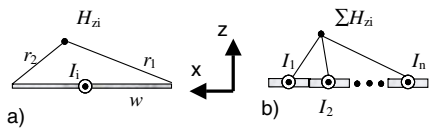

Figure 5. Schematic representation of the thin strip model used in the forward and backward current-to-field calculations. The left picture represents the self-field due to a uniformly distributed current, while the right model gives a non-uniform current distribution as a sum of 'sub-strips'.

Using the same expression (3), we also modelled the tapes as a single strip, i.e. as having a constant lateral critical current distribution, and compared the results with the measured HPMS profile and with the forward calculation using the MK distribution.

2.5. Inverse calculations

The calculation of the inverse problem is based on generation of an inverse matrix relating to the mesh of the currents and the mesh of the measured field data, applying Tichonov regularization; see references [8–12] for details. The number of elements of the calculated J_c^S vector, describing the sheet current distribution that corresponds to the measured HPMS self-field profile, was 25. This number has to be the same as the size of the vector $B_{\text{SF},z}(x)$. Note that this method does not simply yield the best matching result in terms of a least squares criterion, but also discriminates in terms of the fewest possible oscillations in the current distribution vector elements. Thus, the algorithm is robust in the sense that it keeps the solution 'physically feasible' even in the presence of measurement errors and noise.

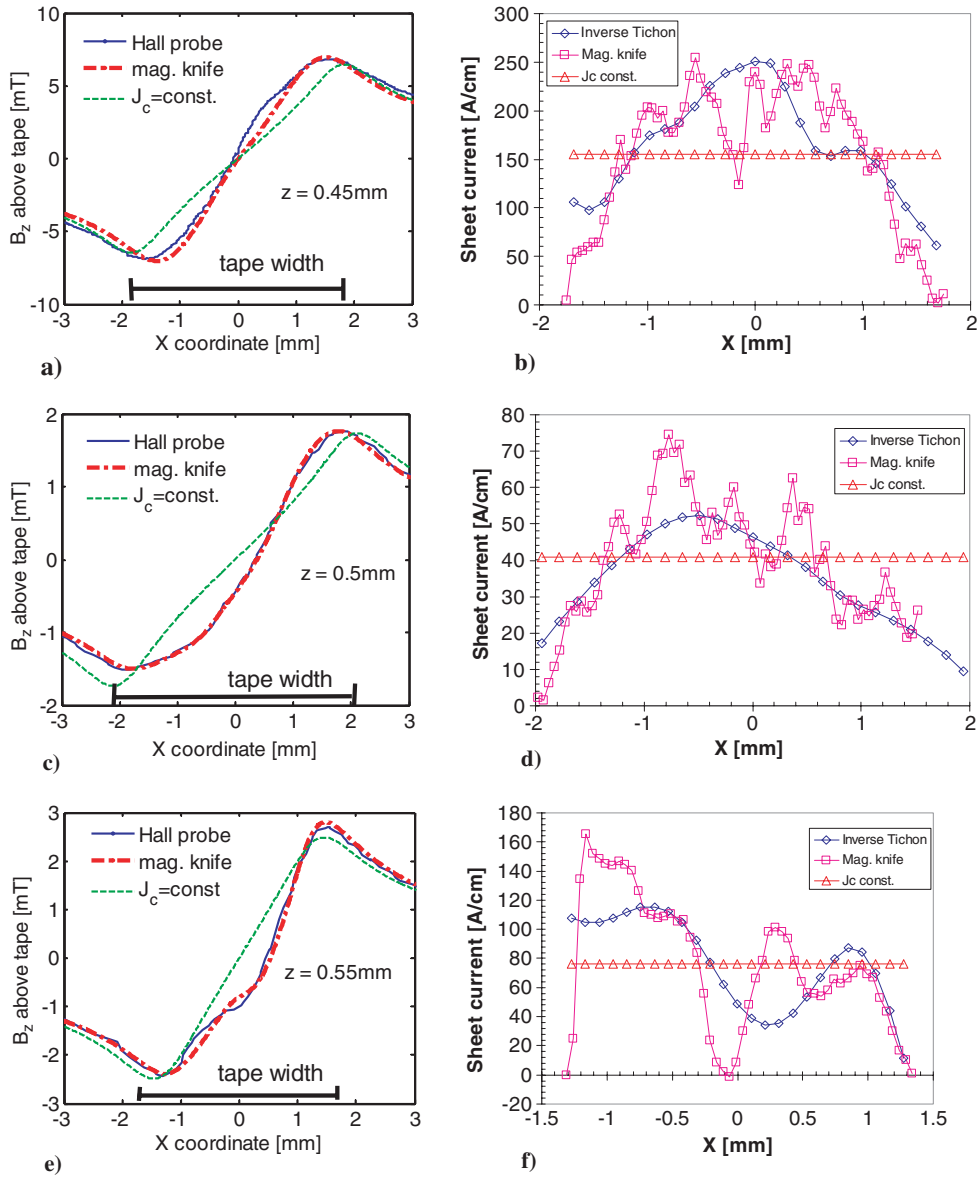

Figure 6. Sample A: (a) the magnetic self-field profiles measured by the HPMS, calculated from the MK current distribution data and calculated assuming a uniform sheet current; (b) the lateral critical sheet current distributions, measured with the MK, calculated from the HPMS self-field data and assuming a uniform sheet current. Sample B: (c) self-field profiles obtained by the HPMS, calculated from the MK data and from assuming uniform current; (d) critical sheet current distributions obtained by the MK, calculated from the HPMS data and assuming uniform current. Sample C: (e) magnetic profiles obtained by HPMS, by forward calculation from MK data and J_c = constant model calculation; (f) local lateral critical current distributions obtained by MK, by inverse calculation from HPMS and J_c = constant model.

3. Results and discussion

As explained in the introduction, the results of the MK and HPMS experiments can be compared in two ways. First, as in [4], we compared the magnetic self-field profiles $B_{\mathrm{SF},z}(x)$ calculated from the MK current distribution with the ones actually measured by the HPMS. These comparisons are shown in figures 6(a), (c) and (e) for tapes A, B and C respectively. Also added (as narrow dashed lines) are the self-field profiles corresponding to a uniform lateral current distribution. Clearly, for all three tapes the HPMS-measured and MK-calculated self-field profiles both deviate significantly from the simple model calculations corresponding to a uniform current distribution. More subtle deviations can be observed between the HPMS and MK profiles.

We can quantify these subtle differences by defining the relative root mean square difference between two self-field profiles as

$$\Delta B_{\mathrm{SF},z} \equiv \sqrt{\frac{\sum_{i=1}^{N}\left(B_{\mathrm{SF},z}^{\mathrm{HPMS}}(x_i) - B_{\mathrm{SF},z}^{\mathrm{MK}}(x_i)\right)^2}{\sum_{i=1}^{N} B_{\mathrm{SF},z}^{\mathrm{HPMS}}(x_i)^2}} \qquad (4)$$

comparing MK with HPMS data and MK with uniform current distribution data, yielding the following. Sample A: $\Delta B_{\mathrm{SF},z} = 8.22\%$ (MK versus HPMS) and 26.33% (MK versus constant model). Sample B: $\Delta B_{\mathrm{SF},z} = 3.14\%$ (MK versus HPMS) and

28.71% (MK versus constant model). Sample C: $\Delta B_{\mathrm{SF},z} = 6.88\%$ (MK versus HPMS) and 27.42% (MK versus constant model).

Compared to the estimated measurement uncertainty of 0.5%, the deviation is significant, especially for tapes A and C, and the best quantitative match is obtained for tape B. It can clearly be seen that the deviation of the constant current distribution model profile is significantly higher compared to MK measurement.

The differences between both experiments are even clearer in the critical sheet current profiles $J_{\mathrm{c}}^{\mathrm{S}}(x)$, comparing the measured MK data with the inverse HPMS calculations and constant current distribution model calculations. These profiles are shown in figures 6(b), (d) and (f). Again, we can quantify the deviations between both datasets in terms of a relative RMS difference

$$\Delta J_{\mathrm{c}}^{\mathrm{S}} \equiv \sqrt{\frac{\sum_{i=1}^{N}\left(J_{\mathrm{c}}^{\mathrm{S,MK}}(x_i) - J_{\mathrm{c}}^{\mathrm{S,HPMS}}(x_i)\right)^2}{\sum_{i=1}^{N} J_{\mathrm{c}}^{\mathrm{S,MK}}(x_i)^2}}. \qquad (5)$$

This gives the following. Sample A: $\Delta J_{\mathrm{c}}^{\mathrm{S}} = 23.71\%$ (MK versus HPMS) and 37.38% (MK versus constant model). Sample B: $\Delta J_{\mathrm{c}}^{\mathrm{S}} = 20.69\%$ (MK versus HPMS) and 39.24% (MK versus constant model). Sample C: $\Delta J_{\mathrm{c}}^{\mathrm{S}} = 36.63\%$ (MK versus HPMS) and 47.38% (MK versus constant model).

The match is better for the tapes A and B with the 'standard' filamentary layout than for the 'columnar' test sample C.

More can be learned from comparing the shape of the self-field and sheet current profiles. In figures 6(a) and (b), one can see that for sample A even the small discrepancies in the magnetic field profile result in clear discrepancies in the current distribution. Yet, the rough shape of the $J_{\mathrm{c}}^{\mathrm{S}}$ profile (maximum in the central part, decrease of the sheet current at the edges) is reproduced by both MK and HPMS.

In sample B, figures 6(c) and (d), the measured and calculated self-field profiles are practically identical and the shapes of the sheet current distribution are remarkably similar (maximum left of centre; gradual decrease towards the right and, just as for tape A, suppression at the edges), especially considering the complexity of experiments.

The columnar filament architecture in sample C is not a standard one, but was realized for model purposes [13]. Figures 6(e) and (f) show that the results of the two experimental methods clearly differ (in particular, the inverse calculation starting from the HPMS data does not yield zero current in between the columns), although both clearly resolve the critical current asymmetry between the left and right columns.

In general, three important conclusions can be drawn. First, in these multifilament Bi-2223/Ag tapes the self magnetic field has only a minor influence on the current distribution. This can be deduced from the fact that more or less the same shape of the lateral current distribution is observed, regardless of the experimental method used (in the MK data the effect of the self-field is negligible, contrary to the HPMS experiment). Therefore, both experiments characterize the intrinsic current distribution and material properties, consistent with the results reported in [14].

Second, discrepancies between MK and HPMS are especially obvious in samples A and C, which have a higher degree of filament bridging. Because of bridging, lateral components of the current become more important and current paths can change significantly depending on the experimental technique used. The relatively good match between HPMS and MK in Sample B thus indicates weak filament bridging.

Third, the assumption of the homogenous current distribution, often used in simple models for the interpretation of AC loss data, is shown to be invalid in typical Bi-2223/Ag tapes. Since the detailed transport AC losses are essentially due to the details of self-field penetration, the comparison between the measured B_{SF} profiles and the ones calculated with a uniform $J_{\mathrm{c}}^{\mathrm{S}}$ show that this assumption might lead to important discrepancies. The shape of the measured current profiles show the main correction to be the intrinsic drop of local current at tapes' edges.

Apart from this extra information obtained by combining the MK and HPMS experiments, the good overall match can be seen as a validation of the experimental and calculation methods. In particular, the data shown in figure 6(d) demonstrate that the inverse calculation method can be used with some confidence to obtain current density profiles from HPMS self-field data. Note that the HPMS method, although indirect, is more versatile than the MK experiment. The MK measures only currents in the immediate vicinity of the local critical current $I_{\mathrm{cm}}(x)$: for lower currents no detectable voltage is generated, while higher currents re-distribute throughout the Ag sheath. In contrast, the HPMS can also be used to measure the distribution of transport currents well below or above I_{c}, as well as DC or AC magnetization currents [8, 9].

4. Conclusions

All investigated Bi-2223/Ag tapes show a significant suppression of the local critical current at their edges. This is not due to self-field effects, but rather an intrinsic consequence of the deformation process. This typical effect invalidates the simple model assumption of uniform critical current distribution, which is often used in the interpretation of AC loss data.

The comparison between lateral current profiles obtained with the direct magnetic knife method and the indirect scanning Hall probe method provides information concerning the importance of lateral current components. Specifically, it can be used to compare the degree of inter-filament bridging between samples.

The HPMS method in combination with the inverse calculation routine proves to be effective and reliable. It is not restricted to critical current measurements only, but can be used in a wide range of temperatures and currents while the speed of the experiment makes it also suitable for measurements in the AC regime. The relatively simple infrastructure, handling and data evaluation make it a technique which is accessible for most laboratories working in the field of superconductivity.

Acknowledgments

The authors acknowledge the financial support from the European Union—ASTRA contract ENK6-CT-2002-80658. The work was also partially supported by projects VEGA 2/5089/25, EFDA/EURATOM FU06-CT-2005-00007, CENG and APVV-51-002305.

References

[1] Bending S J 1999 *Adv. Phys.* **48** 449–535
[2] Grasso G, Hensel B, Jeremie A and Flükiger R 1995 *Physica* C **241** 45–52
[3] ten Haken B, van Eck H J N and ten Kate H H J 2000 *Physica* C **334** 163–7
[4] Kovac P, Masti M, Lehtonen J, Kopera L, Kawano K, Abell S, Metz B and Dhalle M 2005 *Supercond. Sci. Technol.* **18** 1–8
[5] Polak M, Majoros M, Kvitkovic J, Kottman P, Kovac P and Melısek T 1994 *Cryogenics* **34** 805
[6] Smith S W 1997–1999 *The Scientist and Engineer's Guide to Digital Signal Processing* 2nd edn (San Diego, CA: California Technical Publishing)
[7] Kulda J 1974 *Magnetické pole v silnoproudé elektrotechnice* (Praha: Academia)
[8] Usak P 1999 *Physica* C **316** 229
[9] Usak P 2003 *Physica* C **384** 93
[10] Voevodin V V 1977 *Probl. Matemat. Fiz. i Vyc. Mat, Nauka* 91 (in Russian)
[11] Tichonov A N 1965 *DAN SSSR* **6** 163 (in Russian)
[12] Tichonov A N 1965 *Zh. Vychisl. Mat. Fiz.* **4** 5 (in Russian)
[13] Kovác P, Husek I, Melisek T, Metz A, van Eck H J N and ten Haken B 2002 Transport currents in Bi-2223/Ag tapes made by tape-in-rectangulat tube (TIRT) process, current distribution and Ic-stress degradation *Supercond. Sci. Technol.* **15** 624–9
[14] Polak M, Majoros M, Kastler A and Kirchmayr H 1999 *IEEE Trans. Appl. Supercond.* **9** 2151